

A technique for creating linearly stable localized atmospheric features with an application to nonlinear cyclogenesis

Richard Grotjahn*, Daniel Hodyss, Sheri Immel

*Department of Land, Air, and Water Resources, University of California,
One Shields Ave., Davis, CA 95616-8627, USA*

Received 9 December 2001; accepted 1 December 2002

Abstract

A technique is described to construct persistent, three-dimensionally localized features. Localized is used here to signify a structure that is nonzero only in a small region of a larger domain. These features remain nearly coherent and stable in a linear calculation by constructing the local feature from neutral eigenmodes (sometimes called “continuum modes”). The limiting factors are how much the phase speed varies between the modal constituents of the localized feature and how good the match is between eigenvalue and initial-value versions of the governing equations. The governing equations used here are the quasi-geostrophic (QG) potential vorticity (PV) tendency equation. The linear form of the model specifies a zonal mean flow that can have both vertical and meridional shear. The prescribed, mean state has no variation along the flow. The construction of a localized state can be accomplished using fewer modes when meridional shear is present in the zonal mean flow.

The localized features are tested as initial conditions (ICs) in linear calculations and then applied to study a problem in *nonlinear* extratropical cyclogenesis. The nonlinear simulations are not exhaustive. The scope is limited to considering whether nonlinear advection favors nonmodal growth (NG) or normal mode baroclinic instability (NMBI). The applications use several mean flows and IC amplitudes and structures representing conditions prior to observed cyclogenesis. Even though the scope of the application is limited, that scope is better served by using structures that approximate observed traveling, but not developing, localized troughs. The localization includes a procedure that removes linearly unstable normal modes from the IC. Removing the unstable normal modes allows tracking of how quickly growing structures are created by nonlinear advection. Results for selected ICs and basic flows find little NG. Adjacent to the original trough, unstable normal mode-like structures appear soon into the integration. Their properties are more consistent with normal mode growth than NG. Projecting the solution onto eigenmodes finds strong initial amplification of unstable normal modes by the nonlinear terms. The eddies in nonlinear integrations evolve towards a

* Corresponding author. Tel.: +1-530-752-2246; fax: +1-530-752-1793.
E-mail address: grotjahn@ucdavis.edu (R. Grotjahn).

horizontal size that is greater than the linearly most unstable normal mode. Larger initial amplitude leads to faster breakdown of the localization. Emphasis is on ICs with mid or upper tropospheric isolated troughs and sufficient amplitude such that the sum of the IC and mean flow is either an “open wave” or a “closed contour”. The ICs considered develop a leading upper high and trailing lower high and the IC trough develops upstream tilt; both developments are similar to observed cyclogenesis.

© 2003 Elsevier Science B.V. All rights reserved.

Keywords: Baroclinic instability; Nonlinear instability; Quasi-geostrophic model; Localized structures; Cyclogenesis

1. Introduction and motivation

Observed frontal cyclones form and develop in a complex flow that includes other troughs and ridges of varying size, location, and intensity. Our understanding of the development of frontal cyclones is shaped by conceptual and mathematical models. An example of the former is “type B cyclogenesis” (Petterssen and Smebye, 1971) wherein an upper level trough approaches a lower level area of warm advection. When a favorable position is reached that supports growth, the upper and lower features reinforce each other (Hoskins et al., 1985). Most synopticians likely view the interaction between the upper and the lower features to be somewhat localized in space. While the larger environment shapes the properties of the upper and lower trough, each trough does not appear to be one of a long wavetrain of troughs and ridges. In contrast, popular mathematical models (e.g. Charney, 1947; Eady, 1949) for normal mode baroclinic instability (NMBI) tend to examine wavetrains. Similarly, studies (e.g. Farrell, 1984; Grotjahn et al., 1995) of nonmodal growth (NG) develop or start with wavetrain solutions. The primary goal of this study is to describe a procedure by which structures that are nearly stable in a linear sense can be defined that are localized in space. The secondary goal is to demonstrate their use in an application to extratropical cyclogenesis. The principal goal of the application is to assess the relative strengths of NMBI and NG when these stable, localized structures are placed in a nonlinear model. Allowing advective nonlinearity causes the localization to break down. However, the construction of the localized initial condition (IC) creates an experimental situation in which neither NMBI nor NG are favored in a linear sense, so NMBI and NG that may occur are those that advective nonlinear terms favor.

Nonlocalized states are common in theoretical studies due to their mathematical simplicity. The archetype nonlocalized state is a single wavenumber in the along–flow direction. In initial-value studies such as Grotjahn and Tribbia (1995) the lack of localized initial structure leads to rather ambiguous initial conditions. An upper level trough appears to be upstream of one surface low but it is also downstream of an adjacent low due to the use of a single zonal wavenumber in a periodic domain. The procedure described here can remove that ambiguity.

Several studies have examined somewhat localized solutions. One way to create somewhat localized solutions is to introduce zonal variation into the model. That might be done by means of a boundary forcing (e.g. zonally-varying topography as in Grotjahn and Wang, 1990). More commonly, somewhat localized solutions occur in studies of prescribed flows

that have downstream variation such as climatological mean flows (e.g. Frederiksen, 1983). In these studies, the eigensolutions tend to consist of a chain of highs and lows modulated by an amplitude envelope. Another method by which NMBI can be simulated with localized solutions is through the use of solitary wave disturbances (e.g. Mitsudera, 1994). Mitsudera set up two solitary waves: when they resonantly interact, a transition occurs to an unstable structure somewhat resembling a normal mode. Lastly, a strongly nonlinear, isolated vortex has been used to simulate a Gulf Stream ring and hurricane dynamics (e.g. McWilliams and Flierl, 1979; Shapiro and Ooyama, 1990). For example, McWilliams and Flierl (1979) examine ICs with a Gaussian horizontal structure and a two-mode vertical structure in a nonlinear quasi-geostrophic (QG) model. The vertical structure of their IC consists of the barotropic and first baroclinic neutral normal modes. This IC tends to persist with little change in form, however, even in the absence of friction this solution eventually decays through Rossby wave dispersion.

An initial condition consisting of an arbitrarily defined localized structure, will typically develop a spreading packet of waves during an integration forward in time. Some members of the initial packet may be unstable normal modes of a corresponding linear problem. The spread may be in several directions or primarily in one direction such as upstream as seen in Thorncroft and Hoskins (1990, their Fig. 19). The result may be largely diagnosed by projecting the initial state upon the eigenmodes to see which are present and with what amplitude. Simmons and Hoskins (1979) include an analysis of a single trough initial condition in spherical and Cartesian coordinates models. They analyze how this single trough spreads into an ever-widening packet of waves whose edges are related to the maximum and minimum speeds of the prescribed flow. New troughs and ridges appear on the leading and trailing edges of the packet. Over time the new features increase in wavelength and grow at a rate that exceeds and then asymptotes back down to the most unstable normal mode growth rate, presumably due to NG. Wernli et al. (1998) use a localized structure derived from three circular potential temperature anomalies, and then track how the evolution differs between semi-geostrophic and primitive equation versions of their model in the presence of barotropic shear. Swanson and Pierrehumbert (1994) explore nonlinear integrations using a wave packet on a baroclinically unstable jet for the initial condition. The carrier wave has several maxima and several minima. Over time, the leading waves tend to have longer wavelengths while shorter waves appear on the trailing end. This result is similar to linear solutions (Simmons and Hoskins, 1979). Singular vectors using horizontally varying flows also have localized structure (Buizza and Palmer, 1995). More will be said about singular vectors later.

Individual synoptic-scale lows in the atmosphere are not each part of a chain of highs and lows. This conclusion is supported by studies like Grotjahn and Castello (2000) who composite 300 hPa and sea level pressure data for a dozen developing lows. When the data are combined with the origin placed at the center of each trough, one finds no systematic wavetrain of lows upstream or downstream. Instead, the trough starts out isolated and only as it begins to grow do an upper downstream ridge and a lower upstream ridge develop. These adjoining ridges are set up by the vertical motions within the cyclone (Grotjahn, 1996b). A similar pattern develops in nonlinear Eady-type model calculations initialized by a single localized trough (Hakim, 2000). Hakim also interprets his results using singular vectors. A similar evolution is reproduced in a nonlinear quasi-geostrophic model integration starting from a quite localized initial state (Rotunno and Bao, 1996; Fig. 8). The initial state used

by Rotunno and Bao has a vertical trough (no upstream tilt) with weak adjacent highs and lows created by modulating a wavetrain by an inverse distance squared zonal envelope. The envelope they use is not based on the dynamics, so there can be significant projections onto baroclinically unstable modes and also modes of different phase speeds. Such differing speeds can allow nonmodal growth to occur as well. In the application shown here, we use a QG model with fewer approximations than Eady's and we choose our localized initial state based on linear dynamics.

Observations typically reveal that an upper (and perhaps a lower) trough propagates with little or no amplification for one or more days before cyclogenesis commences (e.g. Grotjahn, 1996a). So prior to amplification, the normal mode and nonmodal growth mechanisms (and other things such as nonlinear amplification, downstream energy propagation, and diabatic processes) are either each small or these growth mechanisms are largely canceling. When observed cyclogenesis commences, all of these processes presumably come into play in varying degrees. The scope of our test application is much narrower. Here, an isolated vortex is defined that remains coherent and stable in a linear calculation. The linearly stable vortex is subject to nonlinear advection and so is distorted; more importantly, structures develop from the nonlinear interaction that could release nonmodal instability or excite growing normal modes. In fact, numerous eigenstructures are activated by the nonlinear interaction of the modes comprising the initial and subsequent states. The question addressed by our application is whether normal mode and/or nonmodal baroclinic instability are activated and to what relative degree by nonlinear advection. (Again, each IC has negligible NG and NMBI in a linear calculation.) To limit the scope further, our application emphasizes only a few archetype initial conditions (and amplitudes).

The next section describes the eigenvalue and initial-value models used here. The eigenfunctions are used to construct a localized IC. The third section describes the method of constructing a localized structure. The fourth section describes and analyzes example linear and nonlinear calculations using one or two of these localized structures in an IC. The final section presents a summary and further discussion.

2. Model design

Initial-value calculations are performed using linear and nonlinear forms of a quasi-geostrophic initial-value model. The nonlinear form of the interior QG potential vorticity (PV) equation used here is:

$$\frac{\partial q}{\partial t} + U \frac{\partial q}{\partial x} + \frac{\partial Q}{\partial y} \frac{\partial \psi}{\partial x} + J(\psi, q) = 0, \quad (1)$$

where J denotes a Jacobian and the perturbation QGPV is:

$$q = \nabla^2 \psi + \frac{1}{\rho} \frac{\partial}{\partial z} \left\{ \rho \varepsilon \frac{\partial \psi}{\partial z} \right\}. \quad (2)$$

The boundary conditions in the vertical are:

$$\left\{ \frac{\partial}{\partial t} + U \frac{\partial}{\partial x} \right\} \left(\frac{\partial \psi}{\partial z} \right) - \frac{dU}{dz} \frac{\partial \psi}{\partial x} + J \left(\psi, \frac{\partial \psi}{\partial z} \right) = 0 \quad \text{at } z = 0, z_{\text{top}}. \quad (3)$$

Perturbation stream function is ψ . Upper case letters denote the prescribed basic state where U and $\partial Q/\partial y$ can be functions of z and y . The equations have been made nondimensional using typical scaling magnitudes for horizontal length ($L = 1000$ km), vertical depth ($D = 10$ km), speed ($V = 10$ m/s), and advective time scale ($L/V = 10^5$ s). The parameter $\varepsilon (=f_0 D/\{NL\})^2$ relates L to the Rossby radius of deformation and so is inversely proportional to Brunt-Väisälä frequency N . Density (ρ) and static stability are functions of height (z) only and are chosen to match the [US Standard Atmosphere \(1976\)](#) midlatitude profiles ([Grotjahn, 1980](#), has further details). The model uses Cartesian coordinates on a midlatitude “ β -plane” channel having linear Coriolis variation. This model is hereafter labeled the G model.

The basic wind U reaches its maximum value at the tropopause ($z = 1.0$) and decreases with height in the model’s stratosphere. Two horizontal specifications are tested: no horizontal shear with peak U -values of 1.2 or 3.6 units and a Bickley jet with peak U -value of 3.6 units. Each unit is 10 m/s. No horizontal shear basic flow uses basic state stream function, $\Phi_B = -yU$ while the Bickley jet uses $\Phi_B = -\tanh(y)U$.

These equations are solved numerically as eigenvalue and initial-value problems. Both models are spectral in the horizontal and use second-order finite differences in the vertical. The eigenvalue model assumes complex exponential time dependence, while the initial-value model uses a third-order Adams–Bashforth scheme for time integration. Each model uses 21 vertical levels. All fields are represented spectrally. No horizontal shear calculations use 11 wavenumbers (k) in x and 5 wavenumbers (m) in y for the IC. The Bickley jet cases use 11 wavenumbers in x and 10 in y . The relatively small number of Fourier modes is chosen to simplify the construction of the initial conditions and expedite the eigenvalue model solution. A domain scale is chosen so that the linearly most unstable normal mode occurs at wavenumber 3.

3. Stable localized structure construction

The structures created here are localized in all three space dimensions. Some care is needed in defining a localized feature as an IC. Arbitrarily prescribing an isolated PV maximum in a QG, initial-value model version of the [Eady \(1949\)](#) model (say) results in a solution that quickly decomposes into a chain of highs and lows due to the eigenstructures inherent to that model. Similar dispersal of an arbitrarily defined local structure also occurs in more advanced models. Ironically, it will be shown below that construction of an isolated feature is easier in a model having fewer approximations than Eady’s. All normal modes are unstable in the G model for the wavenumber ranges examined. Numerous neutral eigenmodes also are present; these are labeled continuum modes, following past convention. Since a linearly stable structure is desired, only the continuum modes are used to construct that structure. The continuum mode properties are briefly reviewed, first.

The number of continuum modes is, typically, $NM(NZ - 2)$ at each zonal wavenumber (k) where NM is the number of meridional wavenumbers and NZ the number of vertical levels in the model. If one constructs a stable and coherent structure using continuum modes in the [Eady \(1949\)](#) model, those continuum modes have sufficiently different phase speeds that dispersion causes the local structure to quickly decompose into a chain of highs and lows. When compressibility is included, as it is in the G model, the vertical structures of

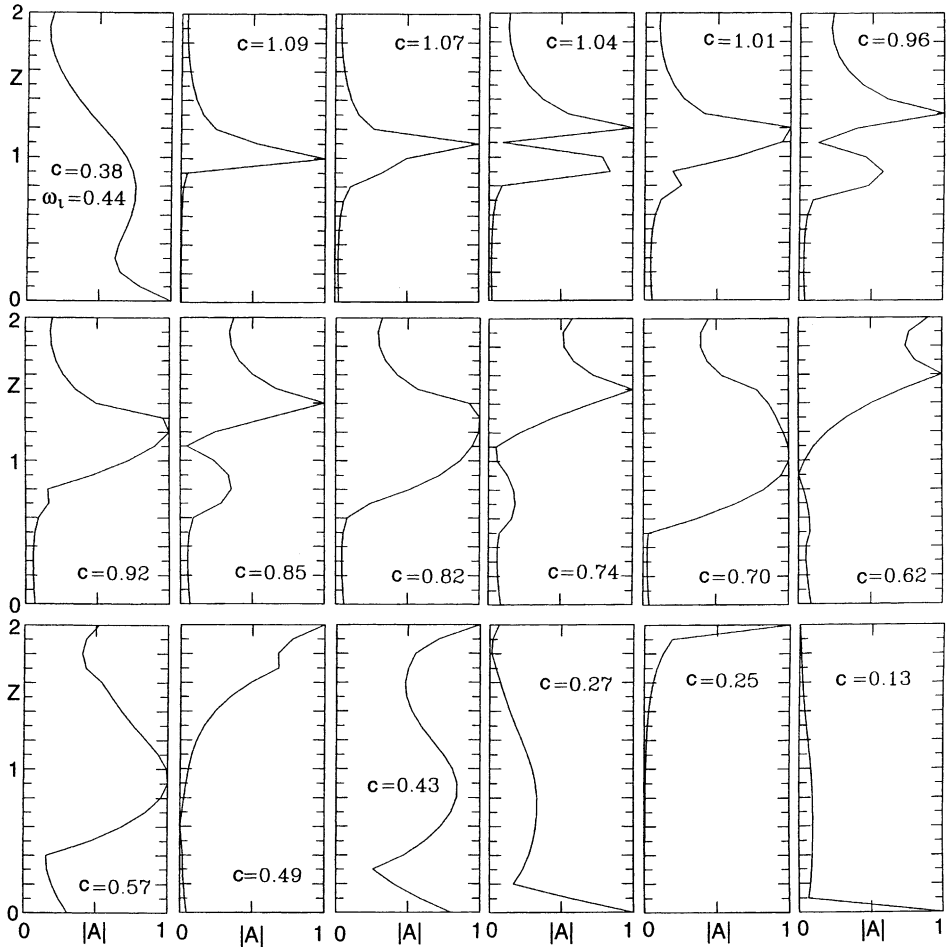


Fig. 1. Amplitude profiles of the growing normal mode (top left corner) and every continuum mode in a matrix eigenfunction analog of the G model at $k = 2.0$. The eigenfunctions are calculated using 21 levels (they are one-dimensional when there is no horizontal shear in the basic flow) for a given meridional and zonal wavenumber. Respective phase speeds for each mode are also given. The growth rate for the normal mode is $\omega_t = 0.44$.

individual continuum modes have greater localization in the vertical (see Fig. 1). The G model is used precisely for this reason.

When there is no horizontal shear, each continuum mode (like each normal mode) has a single zonal wavenumber (k) and meridional wavenumber (m). When the mean flow has horizontal shear, the individual eigenmodes have some localization in the direction along which there is shear. In a jet flow, the eigenmodes tend to have structures oriented along or about that jet. Since the continuum modes for a jet flow themselves have across-flow localization, then modes for a jet flow are more efficient at constructing a localized IC.

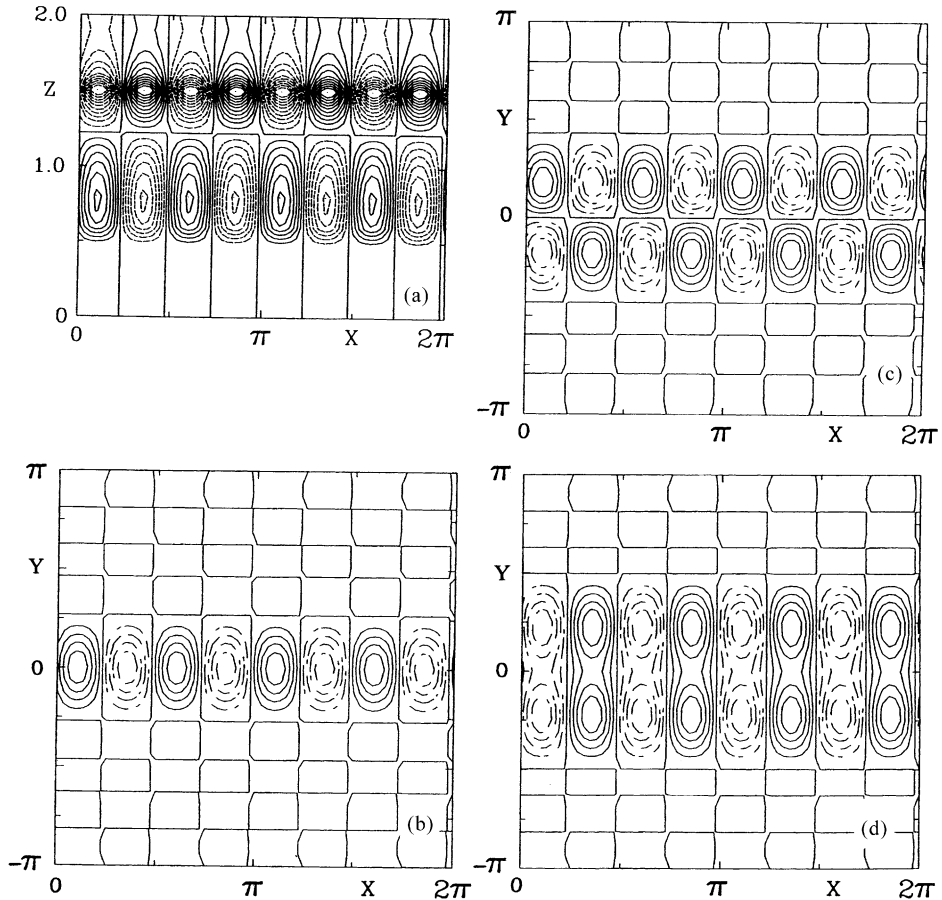


Fig. 2. Example classes of stream function horizontal structures for continuum modes for a Bickley jet centered at $y = 0$ at an upper tropospheric level. Patterns shown are: (a) and (b) mono-polar, (c) dipolar and asymmetric across the jet, (d) symmetric or “camel” dipolar across the jet. (a) A zonal cross-section at $y = 0$ showing the vertical localization, whereas (b)–(d) show horizontal structure.

Bickley jet continuum modes fall into several classes illustrated in Fig. 2. There are continuum mode eigenfunctions that have a mono-polar structure at each zonal wavenumber, k . The mono-polar solutions have a single wavetrain along the axis of the mean flow jet (Fig. 2b). Different modes will have one or more amplitude maxima in the vertical. The faster-moving continuum modes have streamfunction extrema near the tropopause level, where the mean flow is strongest. Slower modes have extrema above or below or both. When Fourier coefficients of an eigenmode are examined, the smallest m has the largest coefficient. The continuum modes with larger dominant m have some type of dipolar structure. Dipolar means there are two wavetrains, one on each side of the jet axis; the wavetrains are commonly opposite in sign and equidistant from the jet (Fig. 2c). The faster-moving dipole continuum modes have wavetrains centered close to the jet axis in the horizontal and vertical. As the

meridional separation between the two primary wavetrains becomes larger, the phase speed drops. Dipole modes are useful to construct efficiently structures that are offset from the jet axis. The vertical structure can be monotonic or have one or more zero crossings in the vertical. So, a monopole or dipole structure is untilted, but it may reverse sign from upper to lower troposphere (Fig. 2a). This combination is handy if one wants a tilted structure constructed from continuum modes. Some continuum modes are “camel dipoles” meaning that they have the same sign for the extrema on opposite sides of the jet (Fig. 2d). These would be useful to construct efficiently broader or narrower modes centered upon the jet. In combination with dipole modes that reverse sign across the jet, one can efficiently construct localized features offset from the jet. In summary, the continuum modes are already localized by the mean flow horizontal shear. This property can be exploited when constructing a localized structure for a mean flow jet.

Each IC is formed from continuum modes. The continuous spectrum in the G model has eigenfunctions with localized vertical structure and similar phase speed at different wavenumbers. For example, Fig. 1 shows vertical profiles of amplitude for the 17 continuum modes (plus the most unstable normal mode) at zonal wavenumber $k = 2.0$ for the eigenvalue problem corresponding to the no horizontal shear, peak $U = 1.2$ units mean flow. The phase speed, c of each mode is indicated as well. The peak amplitude of a continuum mode often occurs at a level where the mode’s phase speed is similar to the basic flow. A similar range of structures is found at other zonal wavenumbers. For longer waves, the localized continuum modes tend to be broader (in the vertical) than those shown in Fig. 1 and vice versa for shorter waves. These properties are used to construct initial conditions that also have localized vertical structure and similar phase speed. Various constructions tested were ICs’ confined near the surface or centered in the upper troposphere. Depending on the target level, the trough may be “shallow” or “deep”. A “shallow” trough is illustrated in Fig. 3d; the “deep” trough (Fig. 3a–c) emphasized here has greater vertical extent and is centered at a lower level. ICs like those shown in Fig. 3 select continuum modes with little range of phase speed and so NG is small in a linear calculation.

The construction of an initial condition when no horizontal shear is present proceeds as follows. The eigenfunctions of a given background flow are found. Next, grouping and then selecting the appropriate members of the continuous spectrum is a straightforward but tedious task. A “target level” is chosen where one desires the IC to have largest amplitude. Next, those members of the continuous spectrum with greatest stream function amplitude near the target level are identified for each zonal wavenumber. At each zonal wavenumber, the member with the phase speed closest to the target phase speed is selected. This target phase speed is initially set to the value of U at the target level. In practice, some adjustment of the target level and target speed is needed to accommodate the properties of the discrete set of continuum modes actually present in the eigenmodel. For example, all continuum modes used to construct the shallow upper trough in Fig. 3d have phase speeds that differ by less than 5%. Further checking is needed since the closest phase speed match may be a mode with undesirable vertical structure. For example, if the first mode chosen may have two maxima in the vertical; in that case the mode with the next closest phase speed match is checked. If the next mode has a single maximum it is selected. At this point one has a selection of continuum modes, one for each zonal and meridional wavenumber combination and these modes have similar phase speed and vertical structure.

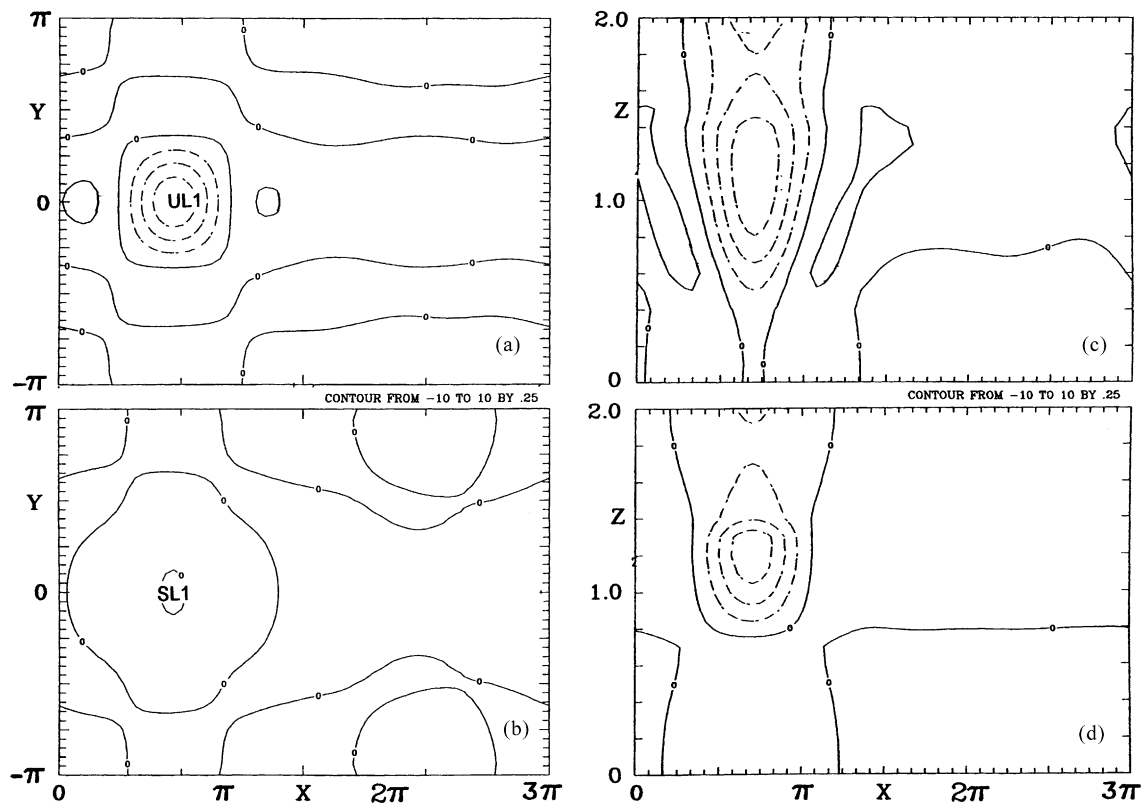


Fig. 3. Initial conditions emphasized in calculations discussed here. Horizontal structure (x vs. y) at (a) tropopause ($z = 1.0$) and (b) surface ($z = 0$) levels for the “deep” IC. Zonal cross-sections (x vs. z) for the (c) “deep” IC and (d) the “shallow” IC. (a)–(d) A basic flow with no horizontal shear. (e)–(h) The Bickley jet basic flow using the “mid” IC with amplitude 3. Horizontal structure (x vs. y) at (e) tropopause ($z = 1.0$) and (f) surface ($z = 0$) levels for the “mid” IC. (g) The sum of the “mid” IC plus Bickley jet at tropopause level. (h) The zonal cross-section (x vs. z) for the “mid” IC at $y = 0$. The labels shown in (a) and (b) are referred to again in calculations shown in Figs. 4 and 6. The labels in (e) and (f) are referred to again in calculations shown in Figs. 7, 8 and 10. The contour interval (0.25 units) is the same in all panels. The labels in (a), (b), (e), and (f) refer to: tropopause level (U), surface (S), and relative minimum (L).

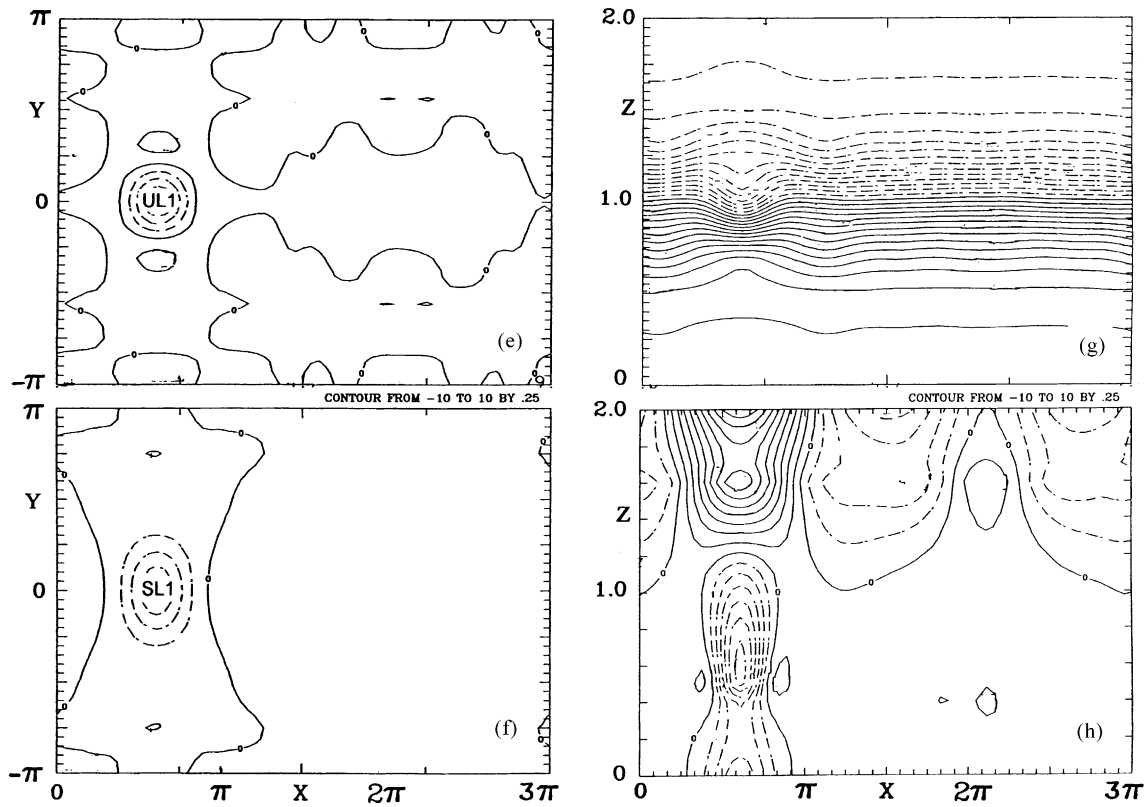


Fig. 3. (Continued).

The localization in the horizontal can be done by several means. A Gaussian in x and y can be decomposed into Fourier coefficients. These coefficients are used as weights for the k and m corresponding to each continuum mode selected above. The result is an IC that is meridionally, zonally, and vertically localized and is comprised of modes having similar phase speed.

An “alternative method” uses Fourier coefficients for a Gaussian in x only. The IC is constructed from continuum modes with meridional wavenumber $m = 0$. To construct the y variation one first multiplies the x and z structure by a Gaussian variation in y . Normal modes having y variation are present in this structure. Unstable normal modes rapidly grow to dominate the solution in test calculations. So, an additional step is employed to filter out these normal modes. The IC is projected onto all the eigenmodes as defined in the numerical model, the amplitude for any growing or decaying normal mode is set to zero, and the remaining projections reconstruct the initial state. The advantage of this IC is that it simplifies the process of constructing the initial state since many fewer continuum modes need be surveyed for use in the IC. The disadvantage is that this IC has more NG since there is no control over the phase speeds of the continuum modes kept to construct the meridional variation. An IC constructed this way therefore has more NG present than if all the constituent modes were chosen to match a narrow phase speed range. In our tests, NG remains small even in the alternative method of constructing the IC.

Constructing the IC for a mean flow jet is much simpler than the method described above if one is satisfied with the localization already present in the eigenmodes. In the Bickley jet application shown below, the 1890 eigenmodes were searched for three properties at each zonal wavenumber k : zero growth rate, phase speed near a target value, and low meridional wavenumber m . The choices were sufficiently distinct that a quick visual inspection of the structure could confirm whether it was a mono-polar mode (e.g. Fig. 2a and b) and that it had the horizontal and vertical localization sought. The ICs shown in Fig. 3e–h were constructed from just 10 continuum modes, one for each k . The phase speeds of these continuum modes increases slowly and monotonically with wavenumber such that the $k = 10$ mode moves 14% faster than the $k = 1$ mode. Results shown here have the basic flow removed. These 10 modes are then weighted as in a Fourier decomposition of a Gaussian exponential in x . Several tropospheric localized structures have been tested, the example emphasized here is shown in Fig. 3e–h. This is labeled the “mid” structure since it reaches its maximum amplitude in the middle and upper troposphere. A “lower” structure has also been tested (not shown). In a linear calculation, the components of the mid structure move with speed six to nine times that of the components of the lower structure. Fig. 3g provides the reader with a sense of how the total streamfunction appears in an archetype case. Fig. 3g shows the combination of “mid” IC with amplitude 3 (arbitrary units) plus the stream function associated with the mean flow Bickley jet at tropopause level.

4. Application to nonlinear advection in extratropical cyclogenesis

4.1. General comments

Extratropical cyclones have favored regions for development. On a surface weather map, cyclones appear to be developing at different rates, not as part of a wavetrain. As stated

in Section 1, composites of typical cyclones (Grotjahn and Castello, 2000) show a single trough, not a wavetrain prior to cyclogenesis; an adjacent high develops as the cyclone intensifies. These properties suggest that it would be appropriate to examine cyclogenesis with a localized structure. Again as stated above, most studies use either an arbitrarily defined localization (which usually quickly breaks down into adjacent developing cyclones and which contains linearly unstable normal modes as well as other modes of various phase speeds) or no localization at all. Our ICs avoid undesirable decomposition into one or more wavetrains that would otherwise result from linear dispersion of constituent modes. This does not mean our ICs are ideal representations of observed conditions prior to cyclogenesis. Observed trough precursors often do generally maintain their coherence, but precursor troughs can have appreciable amplitude, enough so that nonlinearity cannot be neglected. The nonlinear balance in observed troughs that grow slowly may allow linearly unstable constituents, constituents our ICs exclude. Unstable modes (growing and decaying) are excluded because if they are not, these modes tend to rapidly grow and dominate the solution in both linear and nonlinear versions of the model. They no doubt grow rapidly in related studies, such as Hakim (2000). Therefore, the presence of unstable modes obscures the focus of this application upon the role of nonlinear advection in triggering NMBI or NG for an initially localized feature. As such, this application considers just a small aspect of cyclogenesis from a novel perspective.

Each IC is constructed from eigenfunctions arising from a formulation linearized about a prescribed basic flow. So, the basic flow dictates the structures with which one may work. Accordingly, two basic flows are used: one having vertical shear, but no horizontal shear and the other a zonally oriented internal jet. These basic flows illustrate the two archetypes used in most prior linear instability work. The magnitudes of the basic flows are chosen to match winter climatological values.

Results are interpreted using several simple tools since no single tool fully illuminates the relative importance of NMBI and NG. In addition to displaying the perturbation fields as they evolve over time, growth rates of various diagnostics are examined.

Domain-wide integrals of total energy (E) and RMS amplitude (L2 norm) have been used in many prior studies (e.g. Hodyss and Grotjahn, 2001) to help assess the relative importance of normal mode and nonmodal growth in linear studies. These tools have less utility for this study but are kept to provide a point of comparison to other works. During the evolution, individual, adjoining highs and lows appear and the region covered by eddies expands. So, the behavior of individual troughs and ridges can be obscured by the aggregate behavior seen in the global growth rate.

An alternative is to track individual troughs and ridges. Challenges arise when tracking features. The sizes and shapes of the troughs are changing, and the troughs split and merge with other troughs thereby making it arbitrary to identify the area encompassed by a given trough (say) over time. Our solution was to track the values of the perturbation stream function extrema at a single level (similar to what Simmons and Hoskins, 1979 show) as a proxy for an amplitude norm of the individual feature. “Perturbation” refers to that part of the height field when the portion of the height field due to the mean flow has been removed. “Extrema” means the peak values at high and low centers. These extrema growth rates include highs and lows that emerge during the integration as well as those at the start. The extrema are separated into those near the tropopause and those at the surface. An

alternative is to track extrema of vorticity (Müller et al., 1989). The extrema growth rates are only approximate measures of the intensification given the horizontal (and vertical) scale changes that occur. Often, the individual lows and highs start with small scale and expand in all three directions.

To assess the importance of NG is difficult in these simulations because the scale varies over time as well as between the individual features. A broad characterization will be made based on how the growth rates (either of the aggregate or of individual features) compare to normal mode values. Growth rate time series having values exceeding the comparable (in scale) unstable normal mode indicate NG in a linear calculation. Significant NG can be present in a linear calculation for lesser growth rates if the structure differs significantly from the unstable normal mode (i.e. if the emerging normal mode is a tiny fraction of the total perturbation). Here, nonlinear interaction can place amplitude into various modes including unstable normal modes not present at the start. Projecting the total solution onto the eigenmodes illuminates this process.

Calculation of the projection onto the set of normal and continuum modes reveals the amplitudes (and rates of growth) for the eigenmodes during the time integration. Growth rates for key eigenmodes are calculated and separated into contributions from linear growth and (when present) nonlinear forcing. This procedure highlights how nonlinearity triggers and enhances the normal mode instability. As a typical integration proceeds the most unstable modes begin to emerge due to the nonlinear interaction (as are most if not all the eigenmodes).

The governing Eqs. (1) and (3) are separable into tendencies by linear and nonlinear terms. One may project the QGPV onto individual eigenmodes to obtain time series of the modal amplitudes. Thus, a simple formula for the amplitude A_j of the j th normal mode may be written:

$$\frac{dA_j}{dt} = nIF_j + \sigma_j A_j. \quad (4)$$

The growth rate of the j th normal mode is σ_j . The term nIF_j is the contribution to the A_j tendency from the nonlinear Jacobians in (1) and (3); it varies slowly as the flow is distorted.

Each IC is structured to have relatively little change over time in a linear calculation. Consequently, the focus here is upon the nonlinear results, whose evolution depends upon the amplitude assigned. IC construction and nonlinear evolution differ between basic flows with and flows without across-flow horizontal shear. So, a representative example is shown for each type of mean flow. Other ICs and other amplitudes are commented upon, but generally not shown to shorten this presentation.

4.2. Mean flows without horizontal shear

A typical stream function evolution over time is shown in Fig. 4 using the “deep” IC. Early in the nonlinear evolution, the upper level trough develops a NW-SE oriented axis tilt due to the superposition of eddy and basic state winds on the S side of the trough and their cancellation on the N side. In addition, secondary lows and highs appear adjacent to the main trough. The IC has no appreciable trough or ridge at the surface, so growth is more rapid at low levels as troughs and ridges appear and rapidly gain amplitude roughly to match

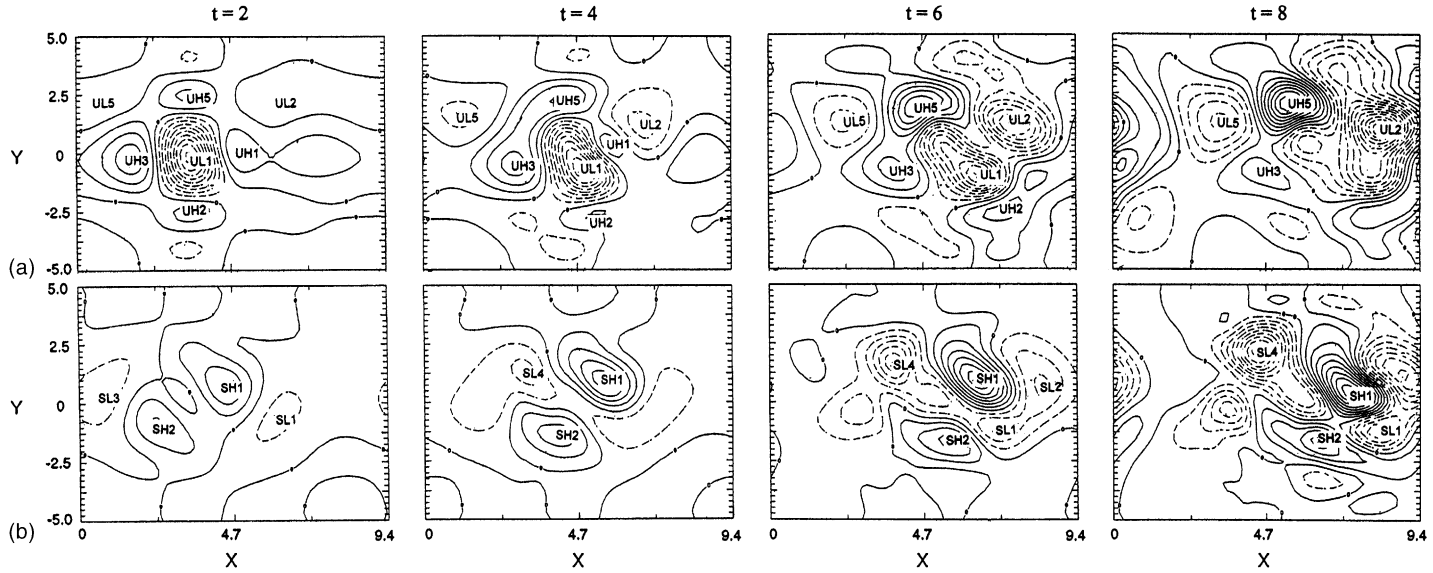


Fig. 4. Contour plots of stream function at times $t = 2, 4, 6$, and 8 during an integration starting from the “deep” trough IC (Fig. 3a–c) on a horizontally uniform basic flow. Evolution at tropopause level is shown in row (a) and surface evolution is shown in row (b). The contour interval (0.1) is the same throughout. Labels refer to: tropopause level (U), surface (S), relative minimum (L), and relative high (H) features. These features are tracked for extrema growth rates shown in Fig. 6.

the corresponding upper feature(s). In contrast, the *original* upper trough (that present in the IC) typically has little amplitude change during the integrations described. For larger amplitude, the distortion of the initial trough shape occurs sooner and adjoining highs and lows grow more rapidly, as well. Several other magnitudes were examined. The other ICs have broadly similar evolution.

Time series of global growth rates for mass-integrated amplitude (L2) and total energy (E) are discussed next. Exponential growth at a constant rate, $\exp(rt)$, would show up as a straight line at value r for the L2 norm. For a normal mode, E grows at twice the rate as the root mean squared amplitude (L2) norm.

The growth rates are compared to the linear normal mode values solely to make a qualitative assessment of the amount of NG occurring. The normal mode values depend on the specified mean flow U . So, the comparison is imperfect since the nonlinear calculations lead to local variations in the shear that presumably increase or decrease the linear instability locally. Also, many wavenumbers are present and the “main” one is difficult to estimate for a localized feature. With those caveats, the width of the upper trough in these ICs is about half the zonal wavelength of the most unstable mode, i.e. the initial trough has similar horizontal scale to the most unstable mode. The most unstable (of all the unstable) normal modes has linear growth rate 0.44 in the basic flow without horizontal shear. Several modes are unstable at each wavenumber. In the linear version of this model configuration, the growth rates spectrum constructed from the most unstable mode *at each wavenumber* has a broad maximum. Other spectra may also be plotted for the second, third, and fourth unstable modes *at each wavenumber*. These other spectra also have broad maxima with their individual peak values at the same wavenumber as the most unstable mode of all. The broad maxima means that the growth rates vary slowly with wavenumber. For example, the growth rates of the four most unstable modes at a wavenumber that is 0.7 times the wavenumber of the most unstable mode of all are only 10–25% less than the growth rate of the most unstable mode of all. Similarly, at a wavenumber 1.3 times the wavenumber of the most unstable mode of all, the growth rates of the top four most unstable modes at this shorter wavelength are only 10–25% less than the rate of the most unstable mode of all. The larger amplitude troughs and ridges that form during the integrations all tend to have wavenumbers within 0.7–1.3 times the wavenumber of the most unstable mode of all. Consequently, our qualitative assessment is that growth rates must be much greater than 0.4 for NG to be considered “large”. NG is at best “moderate” for growth rates within 20% of 0.4 if the growing normal modes are a small fraction of the total solution at that moment. That would be true early on in the integrations shown ($t < 3$ for the no horizontal shear cases). Later in the integrations examined here, projections of the total solutions onto the eigenmodes finds most of the amplitude in several unstable normal modes.

The growth rates are not shown for *linear* integrations of the initial conditions since they remain small during the integration. The eigenmodes hardly interact in the linear model since the relative phase is hardly changing between the constituent modes, so little nonmodal growth is present and each mode individually has zero growth rate. For upper trough ICs tested, the global growth rates remain essentially zero ($< 10^{-4}$) throughout a linear integration. Plots (not shown) of the stream function at various times in the integration mainly show the trough propagating across the domain. The most detectable change is the gradual appearance of adjacent highs and lows along the $y = 0$ axis. The dispersion of

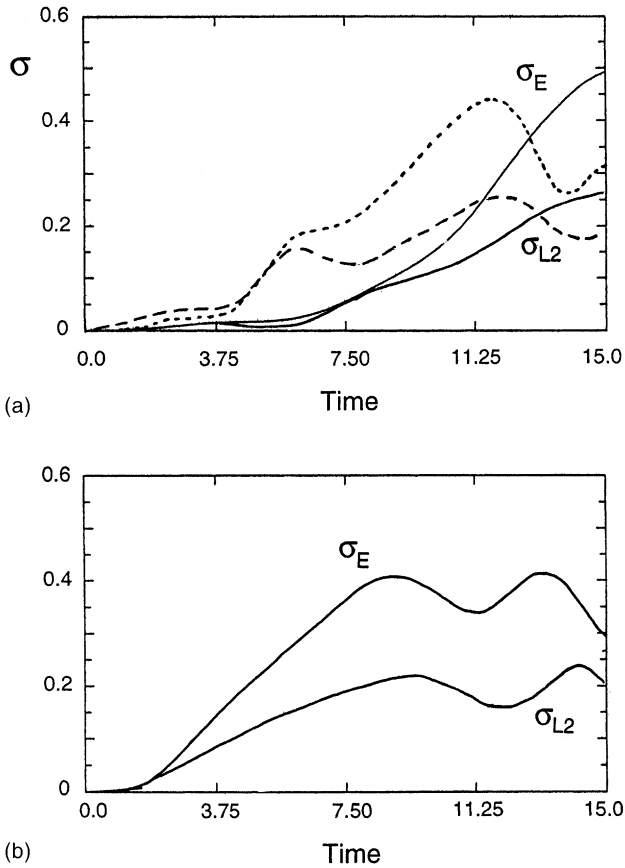


Fig. 5. Time series of global growth rates for the nonlinear calculations using (a) “shallow” IC at two amplitudes and (b) “deep” IC (see Fig. 3). In each case the basic flow is horizontally uniform. E is the total energy integral; $L2$ is the amplitude norm. The solid lines in (a) result from using the IC amplitude shown in Fig. 3d. The dashed lines in (a) are for a run with twice the initial amplitude. The most unstable of all normal modes growth rate is 0.44 for $L2$, 0.88 for E .

amplitude leads to a slow decrease in the peak amplitude of the initial trough. A slight decrease over time of the main trough’s peak amplitude is seen in nonlinear integrations (Fig. 4) as well, though to a lesser extent since unstable modes are also activated. The linear growth rates for ICs constructed by the “alternative method” show more NG since there is a wide spread in the phase speeds of the constituent modes but the NG always remains “small”. Peak values during a linear integration of the alternative method IC briefly reach 0.06 units, with small negative values prevailing during much of the integration (see Fig. 1 in Grotjahn and Hodyss, 1999).

Global growth rates are shown in Fig. 5 for several *nonlinear* calculations using ICs shown in Fig. 3. These growth rates remain small as compared to linear normal mode growth rates based on the flow U . Little growth occurs until after 6 units of time for the standard shallow

IC. When the magnitude is increased the growth occurs sooner. For example, doubling the magnitude of the standard shallow IC leads to E and L2 growth rates exceeding 0.1 units after 4 units of time. Also, for larger amplitudes the time series of E no longer looks like a doubling of the L2 series; for example, L2 global growth *exceeds* E growth for the first ~ 5 units of time using the shallow IC with doubled amplitude (see Fig. 5a). The deep IC has comparable peak values as the standard shallow IC (not shown), but the deep IC develops perturbations more rapidly as seen in Fig. 4. As seen in Fig. 5b, the growth rate exceeds 0.1 after ~ 4 units of time for L2. After 10 units of time E and L2 growth rates oscillate about a value roughly half that of the most unstable mode. However, the perturbation field has highs and lows covering the domain by $t = 10$ and results are no longer applicable to development of a “localized” feature. For the “alternative method” IC, the growth rates time series (not shown) are more regular, matching the linear simulation until ~ 3.5 units of time. After that the growth rates increase smoothly, with little oscillation, up to the most unstable normal mode rate.

Our second measure of growth tracks individual highs and lows. Growth rates are calculated from the extreme values at high and low centers of stream function when the portion due to the mean flow is removed. Instantaneous growth rates are not calculated since they become swamped by amplitude variations created as a center moves between grid points. To avoid this problem, time average extrema growth rates over 0.5 units of time are estimated. These rates are shown in Fig. 6 for selected features of the standard deep IC simulation. The estimates are made for all features that can be unambiguously tracked for at least 0.5 units of time. The main trough in the IC is labeled “UL1” and it is clear that this trough has little growth with time. It is also clear that most surrounding features do not grow with spectacular speed. Rarely does an extrema growth rate exceed the range for normal modes. While NG is very likely present, close inspection of the emerging features finds upstream tilts and comparable amplification at upper and lower levels. The tilts develop over time opposite to what typically occurs for the NG mechanism. For example, UL2 and UL5 in Fig. 4a have companion surface lows (SL2 and SL4, respectively) in Fig. 4b; all of these nearly double in magnitude between times 6 and 8. Lack of tilt change and similar development at all levels are properties more typical of normal mode growth (NMBI) than NG.

For unstable normal modes that tend to dominate the solution, the A_j tendency in (4) is positive and roughly constant due almost entirely to nonlinear forcing. If the mode reaches sufficient amplitude and is strongly unstable in a linear sense, linear exponential growth may dominate. Alternatively, the nonlinear forcing may become negative and partially or greatly negate exponential growth of a particular normal mode by the linear terms.

Table 1 summarizes linear and nonlinear growth rates of three key normal modes for the standard shallow IC integration. The nonlinear forcing activates different normal modes to differing extents. The table illustrates a range of variation over time, also seen in other modes, by tracking the two modes having the largest amplitudes at time 10 as well as the *linearly* most unstable normal mode. For the weakly unstable normal mode (#100) the nonlinear terms dominate throughout the period keeping this mode consistently one of the largest amplitude modes. The nonlinear growth rate declines over time as this mode gains amplitude while the tendency changes more slowly. For the moderately unstable mode (#10) the nonlinear contribution to normal mode growth dominates at the start but quickly diminishes. After time 4, the nonlinear terms are decreasing the amplitude of this mode. So, the nonlinear terms

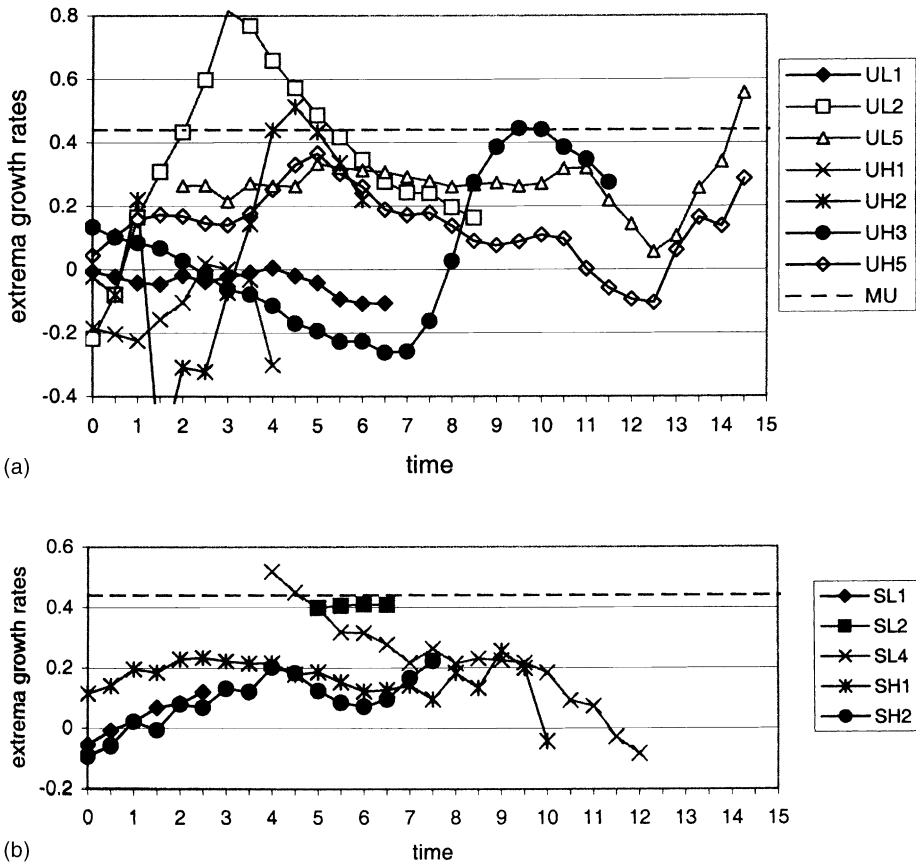


Fig. 6. Growth rates of selected extrema vs. time. (a) Upper and (b) lower levels for the “deep” IC for the horizontally uniform basic flow. The linear growth rate of the most unstable normal mode of them all is 0.44 and is plotted as a dashed line; for scales similar to the troughs and ridges that develop, their corresponding linear normal mode growth rates would be within 10–25% of the most unstable value.

do not always increase the mode over time. A similar effect prevents the most unstable mode (#1) from dominating. At time 5 the nonlinear decay is so strong that the total growth rate for mode #1 is negative. Thus, at time 10 the most unstable mode has only the sixth largest amplitude of the normal modes. The table reveals that a nonlinear growth rate much larger than the normal mode growth rate can be sustained for a long time. For the deep IC many of the same modes are again prominent and a similar wide range of growth rate time series occur.

Similar results are found in some related studies. Pedlosky (1981) shows that nonlinear interaction of weakly unstable modes leads to initially rapid growth by the most unstable mode but that later nonlinear interaction causes that mode to decline in favor of another mode. The favored mode has larger value of a parameter that tends to be larger if the wavelength is greater than the most unstable mode. The most unstable mode is not favored

Table 1

Instantaneous growth rates of selected normal modes for a mean flow without horizontal shear and using the “shallow” IC

Mode #	Property	Time					
		1	2	3	4	5	10
Linear growth rate = $9.03\text{E}-03$ ($k = 0.7, m = 0.9$)							
100	Amplitude	5.67E-02	0.212526	0.431349	0.681857	0.942824	4.287413
	Total	1.96291	0.91219	0.55272	0.38086	0.27328	0.35482
	Nonlinear	1.95367	0.90310	0.54366	0.37182	0.26423	0.34579
Linear growth rate = 0.315331 ($k = 1.3, m = 0.6$)							
10	Amplitude	0.169318	0.367624	0.568212	0.744792	0.889364	3.726187
	Total	1.11099	0.55499	0.33898	0.21219	0.15965	0.27522
	Nonlinear	0.79565	0.23966	0.02370	-0.10314	-0.15568	-0.04010
Linear growth rate = 0.434853 ($k = 2.0, m = 0.3$)							
1	Amplitude	9.81E-03	3.86E-02	7.57E-02	0.10128	9.15E-02	1.474952
	Total	- ^a	0.92399	0.46522	0.11169	-0.29599	0.47658
	Nonlinear	- ^a	0.48911	0.03042	-0.32316	-0.73082	0.04170

Total growth rate (“total”) and that growth rate from just the nonlinear terms (“nonlinear”) are listed. The difference is the linear growth rate for the indicated mode. The two modes with largest projection amplitude (“amplitude”) at time 10 are tracked along with the sequence for the most unstable normal mode. “Mode #” refers to the linear instability rank; the most unstable mode is #1, the 10th is #10, etc.; k and m are zonal and meridional wavenumbers, respectively of the dominant Fourier coefficient. All numbers are nondimensional.

^a Growth rate not calculated.

in our results either. Many favored modes have longer wavelength. For both the shallow and the deep ICs, the 10th, 12th, and 55th most unstable modes (having absolute wavenumbers $\alpha = 1.43, 1.84,$ and $1.48,$ respectively) were favored more than the linearly most unstable mode ($\alpha = 2.02$). The 100th mode (Table 1) is most strongly forced and it has $\alpha = 1.14$. However, a couple of the normal modes favored more strongly than the most unstable mode have smaller scale ($\alpha > 2.02$).

Hakim (2000) tracked the most unstable normal mode in a nonlinear integration of an Eady-type model for a single-vortex IC. He finds growth similar to the linear rate during the first 30 h (~ 1.1 units of time here) and declining thereafter. He also concludes that “nearly all” surface development is from activated growing normal modes. He further anticipates that stronger initial disturbances will shorten the time of development.

Malardel et al. (1993) define ICs for a nonlinear, semi-geostrophic model by introducing “nonmodal” upper level vortices above a frontal zone. What emerges in every case is reportedly the same as when a normal mode is used for the vortex instead.

4.3. Bickley jet solutions

The linear integration for the Bickley jet differs from the linear integration for the mean flow without horizontal shear in the following ways. The solution is not as coherent when the jet is present due to slight differences in the numerics of the eigenvalue and initial-value formulations and to faster eigenmode phase speeds. The linear integration maintains a

single trough quite similar to the IC and propagates it across ~ 5 units distance during the first 3 units of time. A leading upper high first becomes apparent only by time 3. Between 3 and 4 units of time, the single trough begins to split and adjoining troughs and ridges begin to appear. Between 4 and 5 units of time, structures that look like unstable normal modes appear all along the jet: they have upstream tilt, have constant tilt over time, have extrema at the surface and upper troposphere, and move at a slower rate matching the unstable normal modes (instead of the IC trough's faster early speed). The phase speed difference explains the trough split: an unstable normal mode is excited at the start in phase with the IC trough, but since the unstable mode moves slower than the continuum mode components of the IC trough, the IC trough has traveled further than the unstable mode. Hence, the unstable mode becomes visible upstream from the IC trough at a later time, giving the appearance that the IC trough has split. An untilted structure (the IC trough) continues to propagate until $t = 4.6$ units but after that time even it is swamped by growing modes with upstream tilt. Clearly, unstable normal modes are emerging; they become predominant after 6 units of time. For this reason, the nonlinear calculations are halted after $t = 6$, and our interpretation focuses upon the first 3–4 units of time.

A representative example of nonlinear evolution uses the “mid” IC with moderate amplitude ($=3$) and is shown in Fig. 7. As with other nonlinear calculations, highs and lows develop larger horizontal extent (larger than the most unstable linear modes) over time. The total flow should cause the high south of the upper trough in the IC to move counter clockwise around that IC trough. That rotation does not occur because a new low develops on the SE side of the upper IC trough. From $t = 1$ –2, this new low develops then merges with the IC low and the resultant trough is much broader than in the IC. Also from $t = 1$ to 2, a high forms on the SE flank of the high to the N of the upper trough in the IC, leading to a broader high N and E of the (broadened) upper IC trough. At the surface, highs to the W and S of the IC trough develop and merge to form a strong high to the SW of the IC trough. Hence, by $t = 2$, the upper pattern has a single broad trough with a high to the NE while the surface pattern has a single broad trough with a high to the SW. While adjoining highs and lows become more prominent from $t = 2$ to 3, the pattern is predominantly the IC trough with a leading upper high and a trailing surface high. Beyond about 4 units of time, wavenumber 2 dominates the pattern at upper and lower levels. The pattern tends to be more zonally confined and the individual features larger in scale than eddies seen for the horizontally uniform basic flow (compare Figs. 4 and 7). Several other integrations are discussed next for the Bickley jet basic flow.

The expansion of the upper trough in the IC is complex and reveals the emergence of a structure similar to an unstable normal mode from a corresponding linear problem. Those two upper troughs slow down starting at $t \sim 1$ unit while the lower trough continues to move eastward. Close inspection of Fig. 7 shows this process. A more quantitative depiction is given in Fig. 8. From $t \sim 2$ to $t \sim 2.4$ the upper trough does not move. By time $t \sim 2.5$ the upper trough is again moving at a rate to match the lower trough, but the lower trough is now east of the upper. Also, after $t \sim 2.5$ the phase speed is consistently about half the initial speed. Fig. 8 implies the upstream tilt with height increases until $t \sim 2.5$ after which the same tilt is maintained for the rest of the integration. The tilt is quite similar to the most unstable normal mode. When viewed in an along-flow cross-section, the upper

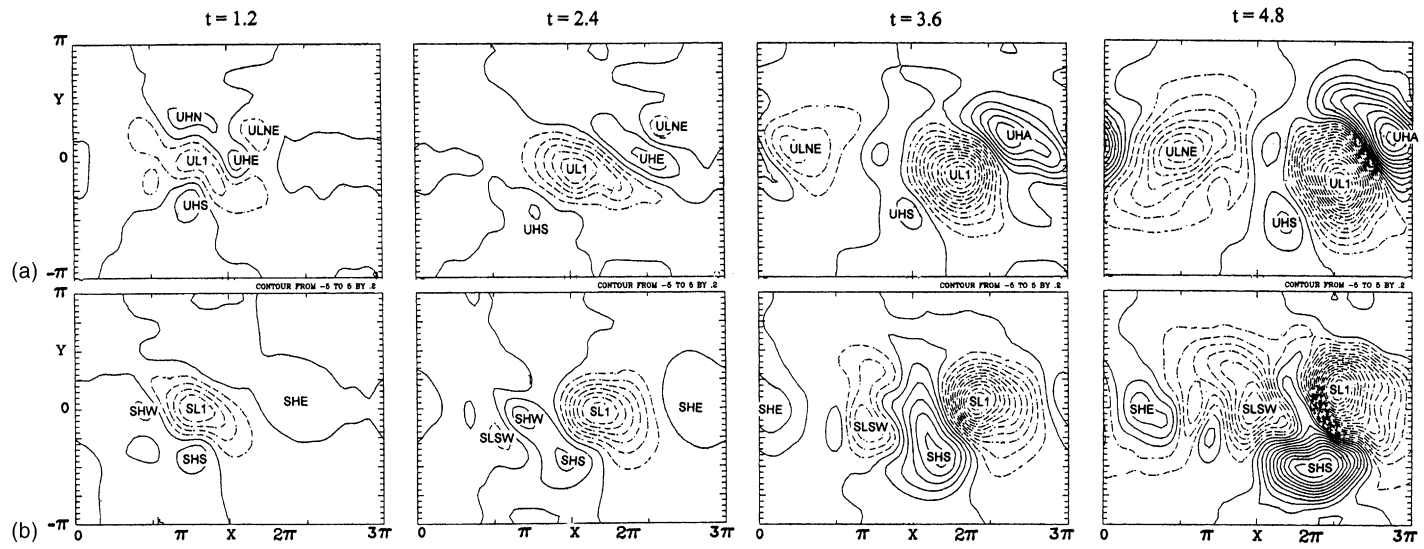


Fig. 7. Similar to Fig. 4. A representative Bickley jet solution is shown at times $t = 1.2, 2.4, 3.6,$ and 4.8 . The “mid” IC (with amplitude 3) shown in Fig. 3e–g is used. Various extrema are labeled to facilitate tracking them between times. These labels are matched with Figs. 3e and f, 8 and 10. The contour interval (0.2) is the same throughout.

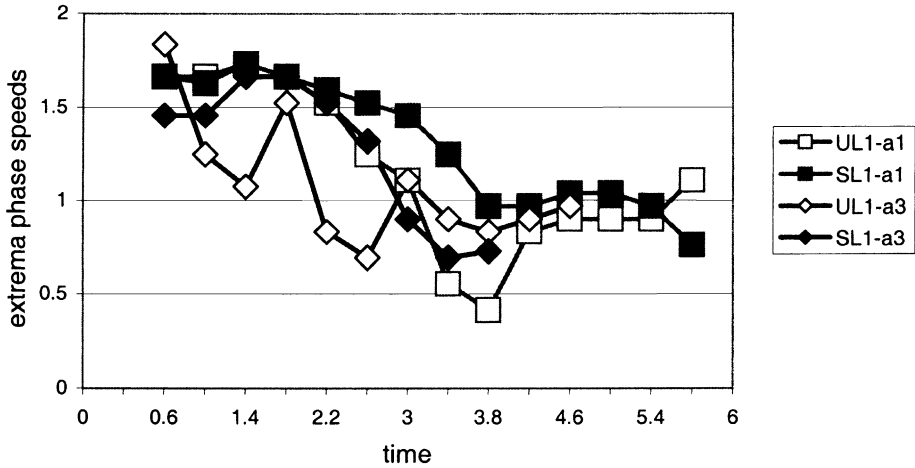


Fig. 8. Phase speeds of the main trough in the IC for two integrations of the “mid” IC on the Bickley jet. Speeds are shown at two levels: tropopause (indicated by “U” labels) and surface (denoted by a “S” labels). Labels that include “a3” have initial amplitude 3 while those with label “a1” have initial amplitude 1. A “Boxcar” moving average over 0.5 units of time is used.

minimum splits; the trailing minimum migrates to a higher elevation than in the mid IC; by $t \sim 4$ the maximum is near tropopause level ($z \sim 1$); the corresponding unstable normal modes have the upper extrema at a similar elevation. During this time the lower trough in the IC has grown more rapidly and consistently than the upper feature so that by $t \sim 3$ the upper and lower troughs have the same amplitude. Hence, while the structure has the phase speed, upstream tilt, and dual extrema (at surface and tropopause levels) of a normal mode, the horizontal scale and the (relative) lower level amplitude are both larger than the corresponding most unstable normal mode.

When a horizontally broader IC is used (still amplitude = 3), highs and lows again develop similar large horizontal extent, however, the nonlinear evolution differs even early on. From $t = 0$ to $t = 1.2$ the upper high on the south side of the IC appears to rotate counter clockwise around to the E side of the upper trough. After $t = 1.2$ this upper high becomes more and more prominent as does a surface high behind the IC trough. By $t = 2$, the upper field is dominated by the IC trough and that high to the E. The lower pattern has highs flanking the IC trough to the E and W. After about $t = 2.5$, the pattern begins to breakdown as several more highs and lows emerge. By $t = 6$, the upper field is dominated by wavenumber 2 while wavenumbers 1 and 2 are strongly present in the lower field. So, the evolution differs, but the two integrations with different IC trough widths evolve into solutions with similar large-scale structure.

When smaller amplitude (=1) is used, the evolution is much more similar for these two IC trough widths. Again, the adjoining development is localized and asymmetric. The trailing surface high and the leading upper high grow the largest first. This property is similar to observed cyclone evolution (Grotjahn and Castello, 2000). Only after $t \sim 3$ units for the narrower and $t \sim 4$ units for the broader IC trough does another adjoining feature have even

half the amplitude of these upper and lower dipoles. The emergence of the normal mode like structure takes longer than for ICs having larger initial amplitude, but the progression of events is similar. In this example, the upper low stops moving from $t \sim 3.2$ to $t \sim 3.6$; after that time the trough maintains upstream tilt and the tilted trough moves at about half the initial speed in the IC.

Additional test runs were made using an analytic, Gaussian-like function defining a single trough IC. This IC has similar structure as the mid IC trough (amplitude = 3), but is not constructed solely from continuum modes. The purpose of this IC is to illustrate what happens when an IC does not have the precise properties of the ICs chosen here: structures with properties like unstable normal modes rapidly emerge. Since those modes are wavetrains, the localization is rapidly lost. Within 1 unit of time the IC trough has upstream tilt and relative maxima at the surface and upper troposphere; both properties are quite similar to an unstable linear normal mode. A leading upper high and trailing surface high also appear and have similar tilt. After 2 units of time, the leading high also has surface and tropopause level maxima and tilt to match the IC trough. Beyond 2 units of time, the zonally-varying (eddy) amplitudes are large enough that nonlinear distortions of the development become quite apparent. (Such “nonlinear distortions” include significant meridional motions of highs and lows by the eddy flow and merging of lows.) Past works using similar analytic function ICs also find quick initiation of the leading upper high and trailing surface high (e.g. [Hakim, 2000](#), for a simpler model; [Simmons and Hoskins, 1979](#), for a more complex model than that used here).

When used alone, the low level IC trough tended to produce smaller scale surface features than did the mid IC; eventually large-scale features appear at upper levels and these would have associated broad scale surface features. This result again suggests the emergence of a mode like an unstable linear normal mode, though as with the mid IC it has larger horizontal scale than the most unstable mode.

When assessing NG for the Bickley jet it is useful to note these properties. First, the unstable normal modes have much larger growth rates than for the no horizontal shear cases. The most unstable normal mode has growth rate 0.81. Consequently, normal modes become a prominent fraction of the total solution sooner than for the integrations using a horizontally uniform mean flow. Also, since the eigenmodes now have localized structure, these modes efficiently define the structure. Fewer modes have large amplitude when the total solution is projected. Most of the few prominent modes are growing normal modes after $t \sim 1$ –2 units. This result is probably general; in a linear study of a basic state jet in spherical geometry, “realistic” ICs strongly projected onto a few unstable normal modes ([Grotjahn and Castello, 2002](#)). So, it is now less valid to assign moderate growth rates (between 0.4 and 0.8) to the NG mechanism.

Global growth rate time series for total energy and amplitude are given in [Fig. 9](#) for the representative “mid” IC. Unlike the deep trough IC but similar to the shallow trough IC for basic flows without horizontal shear, the two time series are quite similar early in the integration. After about 2 units of time the energy growth rate consistently exceeds the amplitude growth rate. From roughly 2.5 to 4.5 units of time the energy rate is twice that of the amplitude rate. Again, energy growth rate is twice the amplitude growth rate for a normal mode. After roughly 5.5 units of time, the domain is largely filled with eddies and both global growth rates decline.

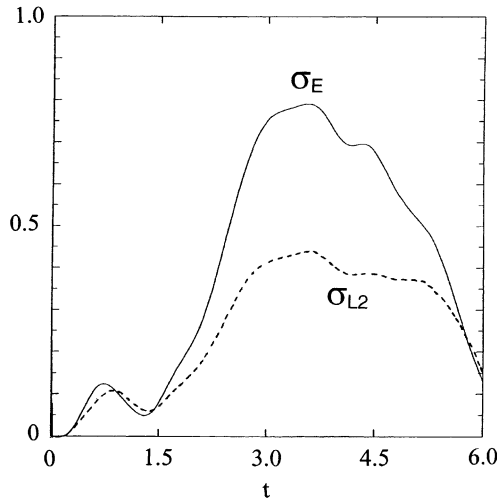


Fig. 9. Similar to Fig. 5 except for the “mid” IC, with amplitude 3, on the Bickley jet. Global growth rate time series are shown of: the total energy (E : solid line) and the amplitude norm ($L2$: dashed line).

Growth rates of extrema at the tropopause and the surface levels are shown in Fig. 10 for the representative “mid” IC. As was the case for basic flows without horizontal shear (Fig. 6) the extrema growth rates rarely surpass the larger normal mode values. Again the growth rates have large fluctuations during the early portion of the integration. At later times

Table 2
Similar to Table 1 except for a mean flow with a Bickley internal jet and using the “mid” IC having amplitude 3

Mode #	Property	Time					
		1	2	3	4	5	6
Linear growth rate = 0.144908 ($k = 0.7, m = 0.5$)							
24	Amplitude	20.7924	26.5987	13.0421	8.8767	56.1627	85.7946
	Total	0.60923	-0.10102	-1.64612	-1.11471	1.00234	0.59510
	Nonlinear	0.46433	-0.24592	-1.79103	-1.25966	0.85745	0.45019
Linear growth rate = 0.617707 ($k = 1.3, m = 0.5$)							
3	Amplitude	19.9974	34.3001	54.4561	75.7415	100.7092	87.9544
	Total	0.83853	0.37778	0.48205	0.257616	0.08382	-0.01305
	Nonlinear	0.22081	-0.23993	-0.13565	-0.360088	-0.53884	-0.63076
Linear growth rate = 0.813358 ($k = 2.0, m = 0.5$)							
1	Amplitude	4.68391	7.8921	18.5062	33.4513	39.7967	16.8461
	Total	0.29689	0.32538	0.76734	0.594323	-0.44223	3.56555
	Nonlinear	-0.60213	-0.57367	-0.13173	-0.304736	-1.34128	2.66649

Total growth rate (“total”) and that growth rate from just the nonlinear terms (“nonlinear”) are listed. The difference is the linear growth rate for the indicated mode. The two modes with largest projection amplitude (“amplitude”) at time 6 are tracked along with the sequence for the most unstable normal mode. “Mode #” refers to the linear instability rank; the most unstable mode is #1, the 24th is #24, etc.; k and m are zonal and meridional wavenumbers, respectively of the dominant Fourier coefficient. All numbers are nondimensional.

(after $t \sim 3$ units) the growth rates are more consistent over time. The IC trough initially decays strongly at upper levels until $t \sim 1.5$ units consistent with a transfer of energy into other modes with differing phase speeds and with the development of similar maxima at surface and tropopause levels. Generally, when features have moderate or larger amplitude (magnitude > 0.4) the growth rates are more consistent. Similar properties are seen in other Bickley jet runs.

Similar to Table 1, growth rates are tracked for individual eigenmodes for the Bickley jet calculations. A representative listing is presented in Table 2 for the mid IC having amplitude 3. The two largest amplitude modes at $t = 6$ are the 24th and 3rd most unstable modes.

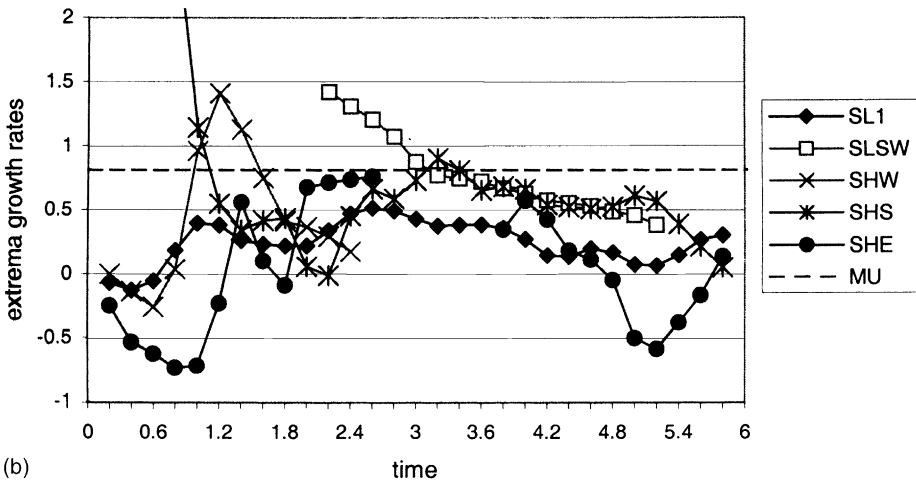
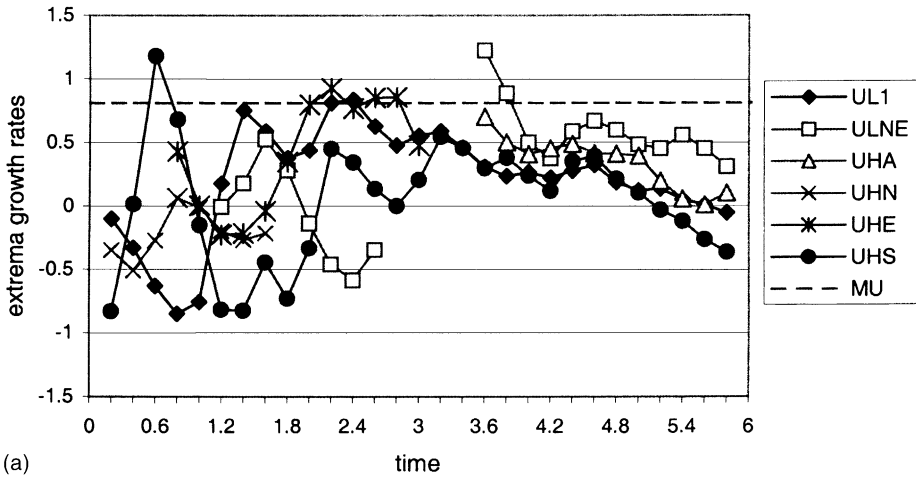


Fig. 10. Similar to Fig. 6 except for “mid” IC with amplitude 3 on the Bickley jet. The growth rate of the most unstable linear normal mode is 0.81 for the Bickley jet used and is plotted as a dashed line. Letter labels refer to features identified in Figs. 3e and f, 7 and 8.

These modes have larger zonal and absolute wavenumber than the most unstable normal mode. The most unstable mode is much smaller at that time, though at some earlier times it is the largest mode. It is clear from [Table 2](#) that the nonlinear forcing of the key normal modes is more variable than for the cases where the basic state has no horizontal shear. Early on, the 24th and 3rd modes have strong nonlinear forcing, but for much of the period these modes are damped by the nonlinear terms. Throughout the period, the most unstable normal mode is damped by the nonlinear terms, at times exceeding the rapid linear growth rate.

Tests using both upper and lower troughs in the IC have similar results as for the mean flow without horizontal shear (not shown). Development was *not* triggered by the upper feature coming into favorable location upstream of the low level feature. (Different initial separations between the lower and “mid” troughs were tried, for close separation development occurred after the “mid” trough had moved past the lower one, for wider initial separation development occurred before the “mid” trough reached the lower.)

5. Summary and discussion

A technique is described by which quasi-stable localized structures are constructed from stable eigenmodes. These structures are tested as IC in linear and nonlinear initial-value models. Mechanisms for development can be controlled in a linear sense by defining an initial feature whose decomposition into eigenmodes: (a) excludes baroclinically unstable normal modes and (b) selects continuum modes of similar phase speed. The ICs tested consist of either a vertically and zonally isolated trough centered near tropopause level, a trough within the upper troposphere, a trough at the surface, or some combination of these structures. The initial state is comprised solely of continuum modes with phase speeds close to a target value. Hence, the resultant structure is localized in all three dimensions and tends to remain coherent when the linear form of the model is integrated forward in time. Since the constituent eigenmodes have very slow relative motion, NG is small. Since unstable normal modes are excluded, NMBI is filtered from a linear calculation. This construct allows examination of the nonlinear term’s contribution to growth. Some applications to basic states having no horizontal shear or having a zonally oriented internal jet are two archetypes of mean flows used in most prior linear instability work. The magnitudes of the basic flows are chosen to match winter climatological values.

Nonlinear advection triggers unstable normal modes when meridional variation of the perturbation is allowed, even if such modes were filtered out of the initial state. Global exponential growth ([Figs. 5 and 9](#)) develops and becomes quite obvious after a few units of model time. The structure of the initial trough becomes distorted ([Figs. 4 and 7](#)) and baroclinically growing eddies appear in the domain. As can be seen in [Figs. 4 and 7](#), eddies form and expand in an irregular way from the initially localized disturbance. So, any limited region chosen to capture any larger amplitude feature will not only be arbitrary, but expanding in size and probably varying in shape over time. To avoid these ambiguities, the development near the trough is examined several ways.

One method tracks the “extrema growth rates” of the peak values for individual lows and highs ([Figs. 6 and 10](#)) similar to [Simmons and Hoskins \(1979\)](#). Almost none of these extrema growth rates exceed the rate of unstable normal modes of comparable scale. When

one does, it does so only briefly and it occurs when the feature first becomes visible on a contour map. Further, these features have properties similar to growing normal modes (companion amplitude changes at different levels, tropopause and surface relative maxima, maintenance of upstream tilt, slower propagation speed). Quantitative evidence is found by projecting the solution onto eigenmodes. The projections reveal that unstable normal modes are found to have significant amplitude when the total solution is projected onto them at various times in the integration. For the Bickley jet fewer than 10 normal modes are dominant after a few units of time.

The normal modes have zero initial amplitude. The nonlinear advection terms dominate normal mode changes at the start: activating those modes, enhancing some modes while suppressing others. The nonlinear terms often prevented dominance by the most unstable (linear) modes and tended to foster the development of larger scale modes (Tables 1 and 2).

The increase of scale is a property of nonlinear development in studies that do *not* localize the solution. Increasing scale is found in weakly nonlinear studies by Hart (1981) and Pedlosky (1981). Numerical simulations allowing full nonlinearity (e.g. Gall et al., 1979; Cehelsky and Tung, 1991; Whitaker and Barcilon, 1995) also obtain solutions with increasing scale. Some studies find that if scale increased then how much it increased depended upon other properties of the model. Using a two-layer model, Whitaker and Barcilon identify nonlinear energy transfers between wavenumbers to be greater at the most unstable wavelength than at longer waves sufficient to make the net growth larger for the longer wave.

Other studies find waves longer than the most unstable favored by mechanisms not present in our model. Welch and Tung (1998) study thermal forcing (of the across-flow temperature gradient by Newtonian cooling) in a two-layer, quasi-geostrophic, “ β -plane” model having just two unstable modes. They conclude that a longer wave can dominate when the heating is too large for the linearly most unstable wave to equilibrate, so that wave breaks and cascades energy to a longer wave which can (since it is less bottom trapped) transfer a greater amount of heat. However, our model does not include any imposed heating. Gall et al. notice that dissipation increases as eddies grow, and since the gradients of a short wave are larger than those of a long wave of identical amplitude, the dissipation increases more rapidly for the shorter waves, thereby favoring longer waves. However, our model does not include any dissipation. Hakim (2000) uses a localized IC, visual inspection of his results finds the primary trough in his nonlinear runs to increase in scale. While Hakim does not discuss scale increase he does comment that larger scale initial conditions have stronger surface development.

The localization of the stream function breaks down in the nonlinear calculations. Adjacent to the initial trough, highs and lows emerge and grow. The emerging eddies may appear somewhat similar to structures that emerge in other studies, such as Figs. 1 and 12 in Simmons and Hoskins (1979). Some readers may view the emerging eddies of that early work as resulting from “downstream development”. However, a more likely explanation is that those adjacent eddies arise from the rapid emergence of unstable normal modes present in the IC used by Simmons and Hoskins. When we do not filter those modes out of our IC, our solutions look more like those in Simmons and Hoskins: a chain of eddies lined up along the axis of the mean flow arises very quickly. “Downstream development” probably does not explain the bulk of the adjacent eddy development in our calculations using *filtered* IC. It is

hard to argue for downstream development when considering our Figs. 4 and 7. The solution shown in Fig. 4 may seem consistent with downstream development in that the upper level feature “UL2” develops more rapidly early in the period (Fig. 6) than other adjacent eddies. However, upstream eddies “UL5” (with its associated “SL4”) have larger growth through the middle of the period (Fig. 6). The Bickley jet solution shown in Fig. 7 reveals that a downstream eddy “ULNE” does grow rapidly through the time period. However, the highs adjacent to the trough in the IC develop consistent with an observed property that follows from the development of a divergent circulation (e.g. Grotjahn and Castello, 2000) and that circulation is not correctly described as “downstream development”. The adjacent high at upper levels is ahead of the trough (“UHA” in Fig. 7) while the adjacent high at the surface is behind the trough (“SHS”). The mixed evidence regarding “downstream development” is one reason why both Figs. 4 and 7 are shown.

It is beyond the scope of this study, but our results may be interpretable in terms of singular vectors. It may be that the initial state projects strongly onto a limited number of singular vectors. The subsequent evolution may thereby be similar. Buizza and Palmer (1995) show how singular vectors asymptote to the most unstable normal modes as the optimization time is increased (and assuming an unchanging mean flow). We note these similarities between their results and ours. First, globally-optimized singular vectors have similar decrease of dominant wavenumber. Buizza and Palmer (1995) show how the peak in the energy spectrum of the singular vector moves towards a lower wavenumber between the initial time and its optimization time. Second, the troughs and ridges in the singular vectors Buizza and Palmer show develop upstream tilt by the optimization time. Third, the horizontal structure can be different at upper and lower troposphere (i.e. different shapes, sizes, and relative locations of the highs and lows between levels). However, two factors argue against the singular vector interpretation. First, Hakim (2000) projects his solution for a localized IC in an Eady-type model onto the singular vectors and concludes that the singular vector decomposition is not as efficient as a normal mode description. Second, the singular vectors also had strong vertical axis tilts at the bottom boundary and fine vertical structure, neither of which is present in applications described here.

A summary of the more important results of our test applications is as follows:

- Growth well in excess of the normal mode values is generally not found in global parameters (Figs. 5 and 9).
- During the integration, highs and lows form adjacent to the localized trough in the IC and these have normal mode-like properties (Figs. 4 and 7). These features have upstream trough axis tilts that they tend to maintain over time (Fig. 8). Their individual growth (as measured using the central value) rarely exceeds a normal mode value of comparable wavelength (Figs. 6 and 10). The adjacent highs and lows tend to develop relative maxima of amplitude near tropopause and surface levels, analogously to normal modes.
- Projecting the solution onto eigenmodes finds that (a) growing normal modes are activated by the nonlinear advection terms, and (b) nonlinear terms inhibit the most unstable mode in favor of other, often larger scale modes (Tables 1 and 2).
- For the Bickley jet, the eigenmode depiction appears very efficient. A small number of eigenmodes has significant amplitude after 1–2 units of time and most of these modes are unstable normal modes.

- Larger initial amplitude leads to faster breakdown of the localization.
- Relative to the trough in the IC, a leading upper high and trailing surface high develop; these highs are subjectively similar to observations (Grotjahn and Castello, 2000).
- The development of the upstream tilt in a localized region as well as the scale change are properties previously noted in singular vector work (Buizza and Palmer, 1995) but work by Hakim (2000) using a simpler, but related model suggests that a normal mode interpretation is more appropriate.

Acknowledgements

This work was partially funded by grant ATM-96-15316 from the National Science Foundation.

References

- Buizza, R., Palmer, T., 1995. The singular-vector structure of the atmospheric global circulation. *J. Atmos. Sci.* 52, 1434–1456.
- Cehelsky, P., Tung, K.-K., 1991. Nonlinear baroclinic adjustment. *J. Atmos. Sci.* 48, 1930–1947.
- Charney, J., 1947. The dynamics of long waves in a baroclinic westerly current. *J. Meteor.* 4, 135–162.
- Eady, E., 1949. Long waves and cyclone waves. *Tellus* 1 (Part 3), 33–52.
- Farrell, B., 1984. Modal and non-modal baroclinic waves. *J. Atmos. Sci.* 41, 668–673.
- Frederiksen, J., 1983. Disturbances and eddy fluxes in Northern Hemisphere flows: instability of three-dimensional January and July flows. *J. Atmos. Sci.* 40, 836–855.
- Gall, R., Blakeslee, R., Somerville, R., 1979. Baroclinic instability and the selection of the zonal scale of the transient eddies of middle latitudes. *J. Atmos. Sci.* 36, 767–784.
- Grotjahn, R., 1980. Linearized tropopause dynamics and cyclone development. *J. Atmos. Sci.* 37, 2396–2406.
- Grotjahn, R., 1996a. Composite trough evolution of selected west Pacific extratropical cyclones. *Mon. Wea. Rev.* 124, 1470–1479.
- Grotjahn, R., 1996b. Vorticity equation terms for extratropical cyclones. *Mon. Wea. Rev.* 124, 2843–2858.
- Grotjahn, R., Castello, C., 2000. A study of frontal cyclone surface and 300 hPa geostrophic kinetic energy distribution and scale change. *Mon. Wea. Rev.* 128, 2865–2874.
- Grotjahn, R., Castello, C., 2002. Nonmodal growth on a sphere at various horizontal scales. *Geophys. Astrophys. Fluid Dyn.* 96, 223–238.
- Grotjahn, R., Hodyss, D., 1999. On initial growth using localized atmospheric vortices. In: *Proceedings of the 12th Conference on Atmospheric and Oceanic Fluid Dynamics* (preprint volume), Columbia University, New York. *Am. Met. Soc.*, pp. 77–78.
- Grotjahn, R., Tribbia, J., 1995. On the mechanism of cyclogenesis as deduced from vertical axis tilts. *Tellus* 47A, 629–637.
- Grotjahn, R., Wang, C.-H., 1990. Topographic linear instability on a sphere for various ridge orientations and shapes. *J. Atmos. Sci.* 47, 2249–2261.
- Grotjahn, R., Pedersen, R., Tribbia, J., 1995. Linear instability with Ekman and interior friction. Part II. Initial value analysis. *J. Atmos. Sci.* 52, 754–777.
- Hakim, G., 2000. Role of nonmodal growth and nonlinearity in cyclogenesis initial-value problems. *J. Atmos. Sci.* 57, 2951–2967.
- Hart, J., 1981. Wavenumber selection in nonlinear baroclinic instability. *J. Atmos. Sci.* 38, 400–408.
- Hodyss, D., Grotjahn, R., 2001. Diagnosing cyclogenesis by partitioning energy and potential enstrophy in a linear quasi-geostrophic model. *Tellus* 53A, 567–577.
- Hoskins, B., McIntyre, M., Robertson, A., 1985. On the use and significance of isentropic potential vorticity maps. *Q. J. R. Meteorol. Soc.* 111, 877–946.

- Malardel, S., Joly, A., Courbet, F., Courtier, Ph., 1993. Nonlinear evolution of ordinary frontal waves induced by low-level potential vorticity anomalies. *Q. J. R. Meteorol. Soc.* 119, 681–713.
- McWilliams, J., Flierl, G., 1979. On the evolution of isolated, nonlinear vortices. *J. Phys. Ocean* 9, 1155–1182.
- Mitsudera, H., 1994. Eady solitary waves: a theory of type B cyclogenesis. *J. Atmos. Sci.* 51, 3137–3154.
- Müller, J., Davies, H., Shär, C., 1989. An unsung mechanism for frontogenesis and cyclogenesis. *J. Atmos. Sci.* 46, 3664–3672.
- Pedlosky, J., 1981. The nonlinear dynamics of baroclinic wave ensembles. *J. Fluid Mech.* 102, 169–209.
- Petterssen, S., Smebye, S., 1971. On the development of extratropical cyclones. *Q. J. R. Meteorol. Soc.* 97, 457–482.
- Rotunno, R., Bao, J.-W., 1996. A case study of cyclogenesis using a model hierarchy. *Mon. Wea. Rev.* 124, 1051–1066.
- Shapiro, L., Ooyama, K., 1990. Barotropic vortex evolution on a beta plane. *J. Atmos. Sci.* 47, 170–187.
- Simmons, A., Hoskins, B., 1979. The downstream and upstream development of unstable baroclinic waves. *J. Atmos. Sci.* 36, 1239–1254.
- Swanson, K., Pierrehumbert, R., 1994. Nonlinear wave packet evolution on a baroclinically unstable jet. *J. Atmos. Sci.* 51, 384–396.
- Thorncroft, C., Hoskins, B., 1990. Frontal cyclogenesis. *J. Atmos. Sci.* 47, 2317–2336.
- US Committee on Extension to the Standard Atmosphere, 1976. *US Standard Atmosphere*. US Govt. Print. Off., Washington, DC, p. 227.
- Welch, W., Tung, K.-K., 1998. Nonlinear baroclinic adjustment and wavenumber selection in a simple case. *J. Atmos. Sci.* 55, 1285–1302.
- Wernli, H., Fehlmann, R., Lüthi, D., 1998. The effect of barotropic shear on upper-level induced cyclogenesis: semigeostrophic and primitive equation numerical simulations. *J. Atmos. Sci.* 55, 2080–2094.
- Whitaker, J., Barcilon, A., 1995. Low-frequency variability and wavenumber selection in models with zonally symmetric forcing. *J. Atmos. Sci.* 52, 491–503.